A finite-element approach to dynamical diffraction problems in reflection geometry

Honkanen, Ari-Pekka

2018-04

Honkanen , A-P , Ferrero , C , Guigay , J-P & Mocella , V 2018 , ' A finite-element approach to dynamical diffraction problems in reflection geometry ' , Journal of Applied Crystallography , vol. 51 , pp. 514-525 . https://doi.org/10.1107/S1600576718001930

http://hdl.handle.net/10138/234485
https://doi.org/10.1107/S1600576718001930

JOURNAL OF APPLIED CRYSTALLOGRAPHY

ISSN: 1600-5767
journals.iucr.org/j

A finite-element approach to dynamical diffraction problems in reflection geometry

Ari-Pekka Honkanen, Claudio Ferrero, Jean-Pierre Guigay and Vito Mocella

J. Appl. Cryst. (2018). 51, 514–525

A finite-element approach to dynamical diffraction problems in reflection geometry

ISSN 1600-5767

Ari-Pekka Honkanen,[a] Claudio Ferrero,[b] Jean-Pierre Guigay[b] and Vito Mocella[c]*

[a]Department of Physics, University of Helsinki, PO Box 64, FI-00014 Helsinki, Finland, [b]ESRF … The European Synchrotron, Grenoble, France, and [c]CNR-IMM Sede di Napoli, via P. Castellino 111, I-80131 Napoli, Italy. *Correspondence e-mail: vito.mocella@cnr.it

Received 11 August 2017
Accepted 1 February 2018

Edited by S. Boutet, SLAC National Accelerator Laboratory, Menlo Park, USA

Keywords: finite-element approach; Takagi…Taupin equations; dynamical diffraction; reflection geometry.

A "nite-element approach to the numerical solution of the Takagi…Taupin equations expressed in a weak form is presented and applied to simulate the X-ray re"ectivity curves, spatial intensity distributions and focusing properties of bent perfect crystals in symmetric re"ection geometry. The proposed framework encompasses a new formulation of the Takagi…Taupin equations, which appears to be promising in terms of robustness and stability and supports the Fresnel propagation of the diffracted waves. The presented method is very "exible and has the potential of dealing with dynamical X-ray or neutron diffraction problems related to crystals of arbitrary shape and deformation. The reference implementation based on the commercial COMSOL Multiphysics software package is available to the relevant user community.

1. Introduction

The Takagi…Taupin equations (TTE) are partial differential equations (PDEs) which describe the dynamical Bragg diffraction in a perfect or deformed crystal (Penning & Polder, 1961; Takagi, 1962, 1969; Taupin, 1964; Authier, 2004; Apolloni et al., 2008). Analytical solutions exist for only a few cases of deformation (Katagawa & Kato, 1974; Litzman & Jarek, 1974; Chukhovskii et al., 1978). In general, one has to resort to numerical solution of the TTE. An approximate approach to solving the diffraction curves of large crystals was introduced recently (Honkanen et al., 2014, 2016), and an iterative method starting from an integral expression of the TTE and involving a series expansion was used by Yan & Li (2014).

Traditionally, the TTE are solved (Authier et al., 1968; Balibar & Authier, 1967; Epelboin & Riglet, 1979; Epelboin, 1985; Gronkowski, 1991; Carvalho & Epelboin, 1993) using a "nite difference (FD) scheme, easily implementable on a Cartesian mesh but not on an arbitrary (e.g. deformed) mesh. In principle, the FD scheme could be implemented on curved crystal surfaces using the reciprocity method (Carvalho & Epelboin, 1998), but this has yet to be done. Furthermore, the incident wave is usually considered to be either a plane wave with reference to an in"nitely distant point source or a so-called •spherical wave• with reference to a point source located on the crystal surface, whereas the intermediate case of an arbitrary "nite distance between the source and the crystal applies to many actual situations (Lagomarsino et al., 2002).

Conversely, a "nite-element method (FEM) based on a weak numerical form of the differential TTE can potentially deal very well with any kind of incident wave and crystals of any shape. A great advantage of this approach is that FEM implementations (Reddy, 2006; Oden & Reddy, 2012) used for

engineering problems are readily available and can be applied to X-ray diffraction problems (Mocella *et al.*, 2003, 2015; Honkanen *et al.*, 2017). One of the bene"ts of using the FEM is that it allows a great deal of "exibility in the selection of discretization, both in the elements that may be used to discretize space and in the so-called basis and test functions. Smaller elements in a region where the gradient of the sought-after function is large could easily be used. Another considerable advantage of the FEM is that its theory is well established, owing to the close relationship between the numerical and the weak formulation of a PDE problem. In the present work, a FEM TTE solver is implemented in a commercial software package (COMSOL Multiphysics; http://www.comsol.com) and the method is veri"ed in the case of Bragg re"ection by perfect and cylindrically bent crystal plates. Bent crystals have frequently been used as focusing elements on X-ray or neutron beamlines in both re"ection and transmission geometry (*e.g.* Tolentino *et al.*, 1988; Chukhovskii *et al.*, 1994; Podorov *et al.*, 2001; Mocella *et al.*, 2004, 2008; Nesterets & Wilkins, 2008; Sutter *et al.*, 2010; Guigay & Ferrero, 2016). The focusing properties of elliptical multilayers have also been studied (Guigay *et al.*, 2008; Morawe *et al.*, 2008; Osterhoff *et al.*, 2013).

The structure of this paper is as follows. We will derive an alternative form of the TTE which is particularly suitable for the FEM at hand in terms of stability and computational ef"ciency. The boundary conditions for the derived TTE are discussed and set in place for re"ection geometry. The propagation of the diffracted wave"eld is examined in the context of Fresnel diffraction. The weak forms of the TTE are derived and the details of the COMSOL implementation are discussed. Finally, the validity of the method is investigated through a chosen set of simulations. This work is a further development of our previously published work (Honkanen *et al.*, 2017).

2. The Takagi…Taupin equations

Let us consider a crystal in Bragg diffraction geometry in which the incident beam is represented by a -polarized (the -polarization case can be described similarly) monochromatic modulated plane wave of the form

$$E_{\rm inc}(\mathbf{r}) = E_{\rm inc}(\mathbf{r})\exp(i\mathbf{k}_0\cdot\mathbf{r}), \quad (1)$$

The length of the wavevector $\mathbf{k}_0$ is $2\pi/\lambda$, where λ is the wavelength of the X-rays. The diffracted wave in air can be written analogously,

$$E_{\rm out}(\mathbf{r}) = E_{\rm out}(\mathbf{r})\exp(i\mathbf{k}_h\cdot\mathbf{r}), \quad (2)$$

where $\mathbf{k}_h = \mathbf{k}_0 + \mathbf{h}$, with $\mathbf{h}$ being the reciprocal vector corresponding to the diffractive planes.

In a non-homogeneous medium, the wave"eld ful"ls the general wave equation

$$\nabla^2 E + k^2(1+\chi)E = 0, \quad (3)$$

of which the solution in the usual two-beam case is of the form

$$E(\mathbf{r}) = E_0(\mathbf{r})\exp(i\mathbf{k}_0\cdot\mathbf{r}) + E_h(\mathbf{r})\exp(i\mathbf{k}_h\cdot\mathbf{r}). \quad (4)$$

For a periodic deformed medium, the susceptibility can be expanded in a Fourier-series-like manner as follows:

$$\chi(\mathbf{r}) = \chi_0 + \sum_h \chi_h \exp[i\mathbf{h}\cdot\mathbf{u}(\mathbf{r})], \quad (5)$$

where $\mathbf{u}$ is the displacement "eld. By multiplying equations (5) and (4) and retaining only the terms relevant to the two-beam case, we obtain

$$\nabla^2 E(\mathbf{r}) = [\chi_0 E_0 + \chi_{\bar h} E_h \exp(i\mathbf{h}\cdot\mathbf{u})]\exp(i\mathbf{k}_0\cdot\mathbf{r}) + [\chi_0 E_h + \chi_h E_0 \exp(-i\mathbf{h}\cdot\mathbf{u})]\exp(i\mathbf{k}_h\cdot\mathbf{r}). \quad (6)$$

Since $E_{0,h}$ vary slowly compared with $\exp(i\mathbf{k}_{0,h}\cdot\mathbf{r})$, their second-order derivatives arising in ∇^2 can be neglected. Hence the following approximation applies:

$$\nabla^2 E \simeq [-2ik_0\,\partial E_0/\partial s_0 - k_0^2 E_0]\exp(i\mathbf{k}_0\cdot\mathbf{r}) + [-2ik_h\,\partial E_h/\partial s_h - k_h^2 E_h]\exp(i\mathbf{k}_h\cdot\mathbf{r}). \quad (7)$$

By substituting equations (6) and (7) into (3), we obtain

$$-2ik_0\,\partial E_0/\partial s_0 = ik^2(1+\chi_0 - k_0^2/k^2)E_0 + ik^2\chi_{\bar h}E_h\exp(i\mathbf{h}\cdot\mathbf{u}), \quad (8a)$$

$$-2ik_h\,\partial E_h/\partial s_h = ik^2(1+\chi_0 - k_h^2/k^2)E_h + ik^2\chi_h E_0\exp(-i\mathbf{h}\cdot\mathbf{u}). \quad (8b)$$

Equations (8*a*) and (8*b*) can be simpli"ed by noting that $k_0^2 = k^2$ and $(k_h^2 - k_0^2) = 2k_h(k_h - k) \simeq 2k\Delta\sin 2\theta_B$, where θ_B is the Bragg angle and $\Delta = \theta - \theta_B$, being the glancing angle of the incident wavevector $\mathbf{k}_0$ on the diffracting Bragg planes.

It is convenient to consider $E_{0,h}(\mathbf{r})$ as the functions $E_{0,h}(s_0, s_h)$ of the oblique coordinates s_0 and s_h along the directions of $\mathbf{k}_0$ and $\mathbf{k}_h$, respectively. As shown in Appendix A, for any function $F(s_0, s_h)$ with gradient ∇F, it holds that $\mathbf{k}_{0,h}\cdot\nabla F = k_{0,h}\partial_{s_{0,h}}F(s_0, s_h)$, where $\partial_{s,h}$ denotes the partial derivative with respect to $s_{0,h}$. Thus, equations (8*a*) and (8*b*) become

$$-2\partial_{s_0}E_0 = ik\chi_0 E_0 + ik\chi_{\bar h}E_h\exp(i\mathbf{h}\cdot\mathbf{u}), \quad (9a)$$

$$-2\partial_{s_h}E_h = ik\chi_0 E_h + 2ik\Delta E_h + ik\chi_h E_0\exp(-i\mathbf{h}\cdot\mathbf{u}). \quad (9b)$$

The case of -polarization can be included in this formalism by replacing the coef"cients $\chi_{\bar h,h}$ by $C\chi_{\bar h,h}$, where $C = 1$ or $\cos 2\theta_B$ for - and -polarization, respectively. By using the notation $c_0 = k\chi_0/2$, $c_{\bar h,h} = kC\chi_{\bar h,h}/2$, $\Delta = k\Delta\sin 2\theta_B$ and introducing the functions

$$D_0(s_0, s_h) = E_0(s_0, s_h)\exp\left[ic_0\frac{s_0 + s_h}{2}\right], \quad (10)$$

$$D_h(s_0, s_h) = E_h(s_0, s_h)\exp\left[ic_0\frac{s_0 + s_h}{2}\right]\exp[i\mathbf{h}\cdot\mathbf{u}(s_0, s_h)], \quad (11)$$

equations (9*a*) and (9*b*) can be written as

$$\partial_{s_0}D_0 = ic_{\bar h}D_h, \quad (12a)$$

$$\partial_{s_h}D_h = i\Delta - \partial_{s_h}(\mathbf{h}\cdot\mathbf{u})D_h + ic_h D_0. \quad (12b)$$

Equations (12a) and (12b) are the most usual form of the TTE. However, for the reasons explained in the next section, it is more convenient to use a modi“ed expression in terms of the functions

$$_0 = E_0 \exp(-i s_h), \quad (13)$$

$$_h = E_h \exp(-i s_h) + ih u. \quad (14)$$

By substituting the above equations into (9a) and (9b), the TTE become

$$\partial_s {}_0 = ic_0 {}_0 + ic_h {}_h, \quad (15a)$$

$$\partial_n {}_h = i c_0 + \partial_n(h u) {}_h + ic_h {}_0. \quad (15b)$$

Equations (15a) and (15b) form the basis of our FEM implementation. The main advantage gained by moving the term out of the equation to the boundary conditions is the increased stability. The reason behind this can be understood by considering equation (12a). At the large limit, the solution of D_h is found to be proportional to $\exp(-i s_h)$, meaning that the phase of the solution oscillates rapidly along the propagation direction of the diffracted beam. On the length scale of the problem, these oscillations even out and thus have little physical consequence. However, they cause a major computational dif“culty. This problem is avoided by moving to the surface term, as s_h varies more slowly along the surface than it would along the direction of the diffracted beam path. Thus, a sparser solving grid can be used, leading to shorter computation times and less heavy memory usage.

3. Boundary conditions for the reflection geometry

The handling of the TTE in x2 is valid for re”ection, transmission and mixed cases. The different cases are separated from each other via the boundary conditions. For simplicity, we focus solely on the re”ection geometry henceforth.

On the entrance surface of the incident wave, the boundary condition for $_0$ is given by

$$_0(r_{surf}) = E_0(r_{surf}) \exp(-i s_{h,surf}), \quad (16)$$

where $s_{h,surf} = s_h(r_{surf})$ is subject to the choice of the origin. For instance, for an incident plane wave $_{inc,plane} = E_0 \exp(ik_0 r)$

$$_{0,plane}(r_{surf}) = E_0 \exp(-i s_{h,surf}), \quad (17)$$

where E_0 is constant in this case. On the other hand, for a divergent source

$$_{inc,div} = \frac{A}{r^{\alpha}} \exp(ikr), \quad (18)$$

where A is a constant and $\alpha = 1/2$ for a line source and 1 for point source. By denoting $r = \overline{SM}$, the position vector of a point M on the crystal surface with respect to the source S, and with being the coordinate perpendicular to k_0 (see Fig. 1), we may use the so-called paraxial approximation

$$kr \simeq k_0 r + \frac{k^2}{2r} + \frac{k^2}{2p}, \quad (19)$$

where p is the distance from S to the origin O on the crystal surface such that the ray $\overline{SO}$ corresponds to the exact incident Bragg direction.

We thus obtain $_{inc,div} \simeq A p^{\alpha} \exp(ik_0 r) \exp(ik^2/2p)$, so the boundary condition becomes

$$_{0,div}(r_{surf}) = A p^{\alpha} \exp\left(ik\frac{^2}{2p}\right) - i s_h. \quad (20)$$

In addition, the boundary condition for $_0$ is left free (i.e. to be solved) on the exit surface of the incident wave and set to zero elsewhere (Fig. 2).

For the diffracted wave $_h$, the boundary condition is $_h = 0$ everywhere else, except on the exit surface where it is left free. Note that the different surfaces may overlap with each other. The different boundaries are illustrated in Fig. 2.

4. Propagation of the diffracted wave

In order to describe the propagation of the re”ected beam in air, we use the rectangular coordinates (s, q) as depicted in Fig. 3. For the solved $_h$, the diffracted wave on the crystal surface is obtained by

$$_{out}(r_{surf}) = _h(r_{surf}) \exp(ik_h r_{surf}) - i s_{h,surf} + ih u_{surf}, \quad (21)$$

with $s_{h,surf} = s_h(r_{surf})$ and $u_{surf} = u(r_{surf})$. Since the diffracted wave is in essence a modulated plane wave, we can propagate it (in the mathematical sense) in the vicinity of the surface simply by adjusting its phase by $\exp(-ik s_h)$.

Figure 1
The nomenclature used in the paraxial approximation.

Figure 2
Boundary conditions for the re”ection geometry. Red denotes the entrance surface of the incident wave, blue the exit surface of the incident wave, red + green the exit surface of the diffracted wave and magenta the boundaries outside the domain of diffraction.

Now, let us consider the plane which goes through the origin ($s_h = 0$) and is perpendicular to s_h. If we propagate $_{out}$ from the crystal surface on this plane, as indicated in Fig. 3, we "nd that

$$_{out;plane}(\ ) = {}_h\, r_{surf}(\ ) \exp\left[i\, s_{h;surf}(\ )\ ih\, u_{surf}(\ )\right]; \quad (22)$$

where $r_{surf}(\ )$, $s_{h;surf}(\ )$ and $u_{surf}(\ )$ are evaluated at r_{surf} with the same coordinate.

Equation (22) allows us to use the Fresnel diffraction integral to compute the wave amplitude far away from the crystal. In a plane at a distance q from the origin, the wave amplitude is

$$(\ ; q) = \frac{1}{(\ q)^{1=2}} \int_{out;plane}(\ ) \exp\left[\frac{ik(\ )^2}{2q}\right] d\ . \quad (23)$$

5. Weak formulation of Takagi…Taupin equations

Following the well established FEM procedure, both sides of equations (15a) and (15b) are multiplied by test functions $v_1(s_0; s_h)$ and $v_2(s_0; s_h)$ and integrated over the domain with the boundary :

$$\int \left(@_{\ } {}_0 \ ic_0\ {}_0 \ ic_{\bar{h}}\ {}_h\right) v_1\, dV = 0; \quad (24a)$$

$$\int \left(@_{\ } {}_h \ i\, c_0 (@_{\ } u) {}_h \ ic_h\ {}_0\right) v_2\, dV = 0. \quad (24b)$$

Let s_0 and s_h be the unit vectors along the directions of k_0 and k_h, respectively. According to Appendix A, we can write

$$v_1 @_{\ } {}_0 = @_{\ }(v_1\ {}_0) \ {}_0 @_{\ } v_1 = r\ (v_1\ {}_0 s_0) \ {}_0 @_{\ } v_1; \quad (25)$$

$$v_2 @_{\ } {}_h = @_{\ }(v_2\ {}_h s_h) \ {}_h @_{\ } v_2 = r\ (v_2\ {}_h s_h) \ {}_h @_{\ } v_2. \quad (26)$$

Utilizing the divergence theorem, we can transform the volume integrals over the divergence terms into the following surface integrals:

$$\int_{\ } r\ (v_1\ {}_0 s_0)\, dV = \int_{\ } v_1\ {}_0 s_0\ n\, dS; \quad (27)$$

$$\int_{\ } r\ (v_2\ {}_h s_h)\, dV = \int_{\ } v_2\ {}_h s_h\ n\, dS; \quad (28)$$

where n is the unit outward normal on . Thus, we "nally obtain

$$\int_{\ } {}_0 @_{\ } v_1 \ ic_0 v_1\ {}_0 \ ic_{\bar{h}} v_1\ {}_h\, dV \int_{\ } v_1\ {}_0 s_0\ n\, dS = 0; \quad (29a)$$

$$\int_{\ } (\ {}_h @_{\ } v_2 \ ic_0^0 v_2\ {}_h \ ic_h v_2\ {}_0)\, dV \int_{\ } v_2\ {}_h s_h\ n\, dS = 0; \quad (29b)$$

where $c_0^0 = c_0 + @_{\ }(\ u)$.

Equations (29a) and (29b) represent the so-called "weak" or "variational" formulation of the differential equations (15a) and (15b). The test functions v_1 and v_2 as well as $_0$ and $_h$ are assumed to belong to an in"nite-dimensional Hilbert space H. It is required that these equalities hold for all test functions in H. In practice, however, the application of the FEM on these functions converts them to functions in a "nite-dimensional function space and then to ordinary Euclidean vectors (in a vector space) that can be managed with numerical methods.

This formulation is called "weak" because it relaxes the requirement expressed by (15a) and (15b), where all the terms of the PDEs must be de"ned at each point (point-wise formulation). The relations in (29a) and (29b), instead, only entail equality in an integral sense. As an example, a discontinuity in the "rst derivative of the solution function does not preclude integration. It introduces, however, a distribution (in a mathematical sense) for the second derivative. Note that, in such a case, equations (15a) and (15b) become immaterial in a discontinuity point.

In contrast with (24a) and (24b), equations (29a) and (29b) do not contain derivatives of the functions $_0$ and $_h$. They can be implemented in a FEM code, using a mesh of two-dimensional elements (often triangles, but rectangles or even higher-order elements are also used) adapted to the crystal shape in quite a straightforward fashion.

The solutions of (29a) and (29b) are expressed as $_0(\ ) = \sum_i {}_{0;i} N_i(\ )$ and $_h(\ ) = \sum_i {}_{h;i} N_i(\ )$, respectively, where the sums go over all n knots in the mesh, and $_{0;i}$ and $_{h;i}$ are coef"cients to be determined. $N_i(\ )$ are the basis (or shape) functions related to the ith knot. Basis functions are nonzero everywhere, except in the vicinity of the knot they are tied to. Customarily, they are polynomial functions (e.g. B-splines) of degree one or higher; in this work quadratic functions were used. The well known Galerkin method (used also in this work) uses a set of test functions identical to the basis functions, i.e. $v_{1;j}(\ ) = v_{2;j}(\ ) = N_j(\ )$. By transforming equations (15a) and (15b) into their weak form, the problem of solving this pair of PDEs is then reduced to solving a system of $2n$ algebraic linear equations from which the coef"cients $_{0;i}$ and $_{h;i}$ are to be determined numerically.

One of the most outstanding assets of the FEM is its ability to choose test and basis functions among a wide host of

Figure 3
The auxiliary planes and coordinate system for computing the wave propagation. In the vicinity of the crystal, the diffracted wave is propagated on the integration plane as a plane wave, from which it is further propagated to the detector plane using the Fresnel diffraction integral.

functions. It is often beneficial to select test and basis functions with a locally variable geometric support. It should be remembered that not all the highlighted features reported above are present in the FD approach, thus potentially making the FD solution of the same problem considerably more laborious and less efficient than the analogous FEM solution.

6. Notes on the reference implementation

The method was implemented in the commercial modelling and simulation software COMSOL Multiphysics 5.3. COMSOL Multiphysics was chosen owing to its widespread use and its readily available structural mechanics and heat-conduction modules that can be used to solve the deformation field for TTE computation in the future development of the method.

The method was implemented using the Weak Form PDE interface, which makes it easy for the user to include arbitrary weakly formulated differential equations into the system. In addition to the strain component included in the TTE, the deformation was taken into account by including the displacement vector field $\mathbf{u}$ into the mesh geometry through the Moving Mesh interface.

Meshing of the crystal domain was done using the Free Triangular mode, which automatically generates an unstructured mesh grid of triangular elements according to the given limitations on element size, etc. The grid parameter of most relevance to this work was the Maximum element size, which limits the maximum distance of the grid nodes. For a simple rectangular geometry, this value corresponds to the typical node separation inside the domain. Later in this discussion we refer to this parameter simply as the (grid) element size.

As Multiphysics uses a Cartesian coordinate system, the oblique coordinates (s_0, s_h) need to be transformed into Cartesian ones. The relation between the two systems is presented in Fig. 4. The unit vectors $\mathbf{s}_0$ and $\mathbf{s}_h$ in the Cartesian basis $\{\mathbf{e}_x, \mathbf{e}_y\}$ are

$$\mathbf{s}_0 = \cos\alpha\,\mathbf{e}_x - \sin\alpha\,\mathbf{e}_y; \qquad \mathbf{s}_h = \cos(\alpha'+\theta)\,\mathbf{e}_x + \sin(\alpha'+\theta)\,\mathbf{e}_y. \quad (30)$$

Thus, the oblique coordinates in terms of x and y are

$$s_0 = \frac{x\sin\alpha' - y\cos\alpha'}{\sin(\alpha+\alpha')}; \qquad s_h = \frac{x\sin(\alpha+\theta) + y\cos(\alpha+\theta)}{\sin(\alpha+\alpha')}; \quad (31)$$

and the partial derivatives are

$$\frac{\partial}{\partial s_0} = \cos\alpha\frac{\partial}{\partial x} - \sin\alpha\frac{\partial}{\partial y}; \qquad \frac{\partial}{\partial s_h} = \cos(\alpha'+\theta)\frac{\partial}{\partial x} + \sin(\alpha'+\theta)\frac{\partial}{\partial y}. \quad (32)$$

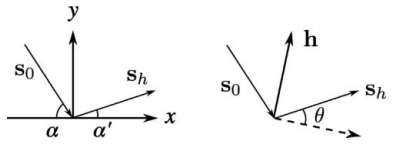

Figure 4
Direction vectors $\mathbf{s}_0$ and $\mathbf{s}_h$ of the incident and diffracted waves with respect to the Cartesian coordinate system (x, y). The sign convention is so that both angles are positive for the case depicted. Note that the coordinate system is not, in the general case, aligned with $\mathbf{h}$.

Table 1
Crystal parameters and diffraction-related quantities for symmetric Si(111) at a photon energy of 6 keV (σ-polarized).

χ_0	$0.274564\times10^{-4} + i\,0.109657\times10^{-5}$
χ_h	$0.109980\times10^{-4} - i\,0.991441\times10^{-5}$
$\chi_{\bar{h}}$	$0.991441\times10^{-5} + i\,0.109980\times10^{-4}$
Bragg angle θ_B	19.24°
Interplanar distance	3.14 Å
Absorption length	29.99 μm
Darwin width	9.83×10^{-5} (47.7 μrad)
Extinction depth	0.73 μm
Extinction length	2.22 μm
Refraction correction	9.12×10^{-5} (44.2 μrad)

For the propagation calculations, the solved complex wave amplitudes on the crystal surface are exported into a text file. A program written in Python is used to read the contents of the files and compute the Fresnel integral for all points on the detector plane.

7. Simulations

In order to validate our FEM method, we solved the TTE for the symmetric Si(111) reflection for undeformed and cylindrically bent crystals for various incidence angles. The energy of the σ-polarized incident X-rays was set to E = 6 keV. The $\chi_{0;h;\bar{h}}$ values, together with diffraction-related quantities, were computed with XOP 2.4 (Sanchez del Rio & Dejus, 2011; Sanchez del Rio *et al*, 2015) and are presented in Table 1.

7.1. Reflectivity curves of the undeformed crystal

The TTE were solved for various incidence angles for an undeformed rectangular crystal slab. The thickness of the crystal was set to 50 μm. In order to avoid disturbances caused by the sides of the crystal, the incident plane wave of equation (16) was multiplied by a Gaussian window function. The full width at half-maximum (FWHM) of the window was chosen to be 100 μm. Note that this FWHM applies for the amplitude of the wave; for the intensity of the wave, the given value should be regarded as the full width at a quarter of the maximum (FWQM). The width of the crystal was chosen to be 200 μm, which accommodates the masked beam well. For the aforementioned parameters, the simulated crystal can be considered thick in terms of the diffraction.

The reflectivity or rocking curves (RCs) were solved using maximum triangular element sizes of 0.5, 1, 1.75 and 2.5 μm (Fig. 5). As expected, the result converges towards the reference curve computed with XOP as the element size gets smaller. The largest effect of the grid density can be seen on the top of the curve. This is natural, since this is the region of the RC where the dominating length scale is the extinction length. Compared with the extinction length of 2.22 μm, we find that the grid size needs to be two or three times smaller in order to obtain satisfactory convergence.

The deviations seen in the tails of the RCs for the 1.75 andin the boundary condition of $_0$. Using Bragg•s law, the phase 2.5mm grids arise from the oscillating phase factor ðexp s_hÞ